Adsorption (2014) 20:477–481
DOI 10.1007/s10450-013-9581-9

Highlights of non-equilibrium, non-isobaric, non-isothermal desorption of nitrogen from a LiX zeolite column by rapid pressure reduction and rapid purge by oxygen

V. Rama Rao · S. W. Chai · M. V. Kothare · S. Sircar

Received: 4 March 2013 / Accepted: 20 September 2013 / Published online: 24 October 2013

Abstract The effects of adsorption kinetics, column pressure drop, gas phase mass and heat dispersions, gas–solid heat transfer resistance, and adsorber adiabaticity on desorption of N_2 from a LiX zeolite column by O_2 purge as well as pressurization–depressurization of the column using pure N_2 were recently studied using a numerical model of these processes [Chai et al. in Ind Eng Chem Res 50:8703, 2011, Chai et al. in Adsorption 18:87, 2012, Chai et al. in AIChE J 59:365 2013; Rama Rao et al. in Adsorption 2013]. The role of adsorbent particle size and column length to diameter ratio in determining the durations and efficiency of these processes were also investigated. These studies revealed several important limiting and optimum conditions for optimum operation of these processes which can be useful in design of a practical rapid pressure swing adsorption (RPSA) process for medical oxygen concentrator (MOC) application. The purpose of this short review article is to consolidate and re-emphasize these important results in a single article to be used as a guideline for design of a RPSA-MOC unit.

Keywords Non-equilibrium · Non-isobaric · Non-isothermal · Rapid pressurization and depressurization · Oxygen purge · LiX zeolite

1 Introduction

The rapid pressure swing adsorption (RPSA) cycles for a medical oxygen concentrator (MOC) design generally use some variations of the Skarstrom cycle (1960) consisting of (a) selective adsorption of N_2 from compressed air in a zeolite column to produce the O_2 enriched product gas (b) desorption of N_2 by pressure reduction of the column (c) further desorption of N_2 by back purge of the column with a part of the product O_2, and (d) pressurization of the column with compressed air or a part of the product gas or both. LiX zeolite is the preferred choice for air separating adsorbent [Leavitt 1991]. The total cycle times (t_c) for most of these processes are approximately 10 s or less [Chai et al. 2011] and the key process performance variables are the product O_2 purity, the bed size factor (BSF) defined by the total amount of adsorbent in the RPSA system per ton per day of contained O_2 product rate, and the O_2 recovery (R) defined by the amount of O_2 product per unit amount of feed O_2 per cycle. Lower BSF (smaller adsorbers) and larger R (smaller air compressor and power) are the desired design goals.

A common approach to reduce the BSF of a RPSA process for a MOC is to increase the cycle frequency by reducing t_c. However, t_c cannot be decreased indefinitely to reduce the BSF due to the impeding effects of finite mass, heat, and momentum transfer resistances within an adsorber. This important point was recently demonstrated experimentally by operating a very small, single column adsorber packed with LiX zeolite particles to produce $\sim$90 % O_2 product from compressed synthetic air. (79 % N_2 + 21 % O_2) (Chai et al. 2011). Figure 1 reproduces a cyclic steady-state data set from this study showing the BSF as a function of t_c for an adsorption pressure of 3 atm and a final desorption pressure of 1 atm and using two different adsorbent particle sizes. The Figure shows that a minimum BSF of $\sim$50 lbs/TPD$_c$ O_2 can be produced in the t_c range of $\sim$2.5–6.0 s. The BSF increases if t_c is further reduced. This value of BSF is less than that of other published RPSA process data (Chai et al. 2011, 2012).

V. Rama Rao · S. W. Chai · M. V. Kothare · S. Sircar (✉)
Department of Chemical Engineering, Lehigh University, Bethlehem, PA 18015, USA
e-mail: sircar@aol.com

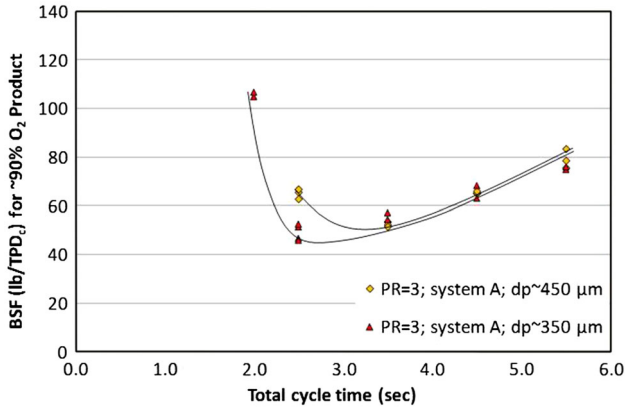

Fig. 1 BSF vs t_c for different particle sizes

It follows that the times of the individual steps of a Skarstom-like RPSA cycle must be <1 s, preferably <0.5 s, in order to accommodate them within an optimum total cycle time of ≤6 s. Consequently, the effects of various previously mentioned transport resistances on the efficiency of very fast operation of these individual steps may be critical.

This paper highlights the key findings of a numerical simulation study of these effects using a detailed non-equilibrium, non-isothermal, non-isobaric mathematical model describing transient dynamics of an adsorption column (Chai et al. 2012; Rama Rao et al. 2013). The model assumes that (a) the adsorber is adiabatic (b) the gas-solid mass and heat transfer coefficients are finite, and (c) the column pressure drop and mass and thermal dispersions in the gas phase are present. Literature correlations were used to estimate adsorbate mass transfer coefficients based on a linear driving force model (Ruthven 1984), axial gas phase mass and thermal diffusivities (Ruthven 1984), gas–solid heat transfer coefficients (Wakao et al. 1979), and column pressure drop (Ergun 1952). A published empirical correlation was used to describe pure and mixed gas adsorption isotherms of N_2 and O_2 on LiX zeolite (Rege and Yang 1997).

2 Model simulations and results

We simulated (a) desorption of N_2 from a LiX zeolite column by rapid purge with O_2 because the quantity of product back purge in a RPSA-MOC unit is a critical and sensitive variable in establishing the BSF and R (Chai et al. 2012), and (b) times required for completion of pressurization-depressurization steps for a LiX zeolite column because they are important in determining the over-all cyclic frequency of the process, hence, the BSF. Idealized representative models were used to mimic both cases.

2.1 Desorption of N_2 from LiX zeolite by rapid O_2 purge (Chai et al. 2012, 2013)

An adsorber (Length = L; Diameter = D) was packed with LiX zeolite particles (diameter = d_p, total weight = W) was initially equilibrated with pure N_2 (1 atm, 298 K) and then purged with pure O_2 introduced into the column at 298 K. The gas pressure was sufficient to overcome the column pressure drop so that the effluent gas was at ambient pressure. The amount of purge gas needed to remove a certain fraction (f_{N2}) of total N_2 (adsorbed + void) initially present in the column was estimated for different purge durations (or inlet gas flow rates) using different L/D ratios (same W) and d_p.

The minimum specific amount of purge gas ($\bar{Q}^*_{O_2}$) for a given desorption duty (f_{N2}) is exhibited for isothermal and isobaric desorption where instantaneous mass and thermal equilibrium is attained between the gas and solid phases in the column. The amount of purge gas ($\bar{Q}_{O_2}$) for the same desorption duty will be higher for adiabatic, non-isobaric desorption with finite transport resistances. We define an inefficiency of desorption by a variable θ $\left[= \bar{Q}_{O_2}/\bar{Q}^*_{O_2} \geq 1\right]$. Clearly, $\theta = 1$ represents the most efficient desorption by purge case.

Figure 2 shows three sets of histograms for θ which were generated using $W \sim 170$ g, $d_p = 400$ µm, and $f_{N2} = 0.85$ (base case conditions). The left set of histograms was generated for $L/D = 1.39$ (regular adsorber) and a desorption time of ~2 s in conjunction with sequential introduction of various non-idealities in the simulation model [B: +adsorption kinetics, C: +gas phase dispersions, D: +pressure drop, E: +adiabatic column operation, F: +gas–solid heat transfer resistance]. The progressive increase of θ due to column adiabaticity and transport resistances is clearly demonstrated. Finite adsorption kinetics, column pressure drop, and non-isothermal operation contribute most to increase θ, while the effects of gas phase dispersions and finite gas–solid heat transfer resistance are relatively small. It should be noted that nearly 50 % more purge gas is needed over the minimum amount when all resistances are included. The middle set of histograms show that the non-idealities have similar relative effects when a pancake adsorber design ($L/D = 0.18$) was used under same conditions as before except that the detrimental effect of column pressure drop was reduced. About 40 % more purge gas is needed than the minimum amount when all resistances are included for this case. The right set of histograms was generated using $L/D = 0.18$ and different purge times while including all resistances. The purge inefficiency increases drastically ($\theta > 2$) when its duration is significantly lowered, primarily due to higher pressure drops caused by higher purge gas flow rates.

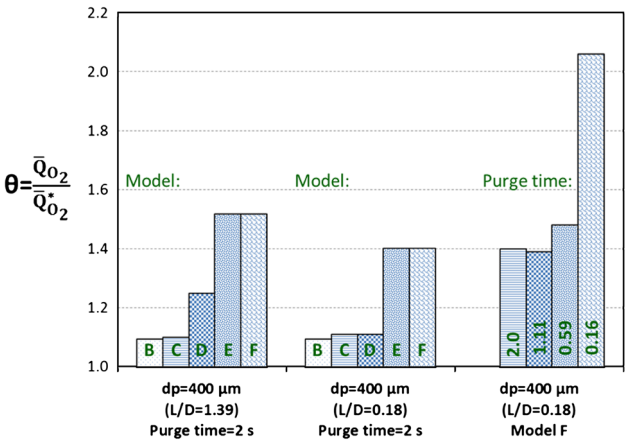

Fig. 2 Influence of various resistances on purge inefficiency

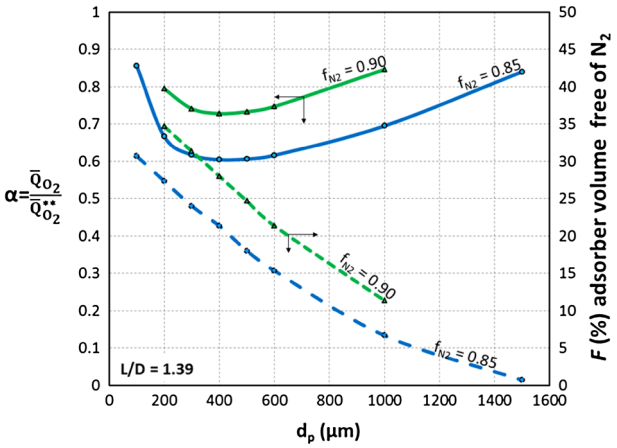

Fig. 3 Purge inefficiency vs d_p

Figure 3 shows a set of plots of another inefficiency variable α [$= \frac{\bar{Q}_{O_2}}{\bar{Q}^{**}_{O_2}}$] as functions of d_p for two different values of f_{N2}, where $\bar{Q}^{**}_{O_2}$ is the specific amount of purge O_2 required to remove 99.98 % of N_2 from the column under ideal conditions of desorption by purge. Figure 3 also shows the fraction of the adsorber volume (F) that is free of N_2 in the purge gas introduction end at the end for a given desorption duty. Larger F is desirable for efficient desorption process (Chai et al. 2012). The Figure demonstrates that (a) there is an optimum particle size range ($\sim$300–600 μm) where α exhibits a relatively flat minimum, and (b) F can be impractically small for larger particle sizes (>1,000 μm) when $f_{N2} < 0.9$.

2.2 Rapid pressurization-depressurization of a LiX zeolite column (Rama Rao et al. 2013)

The effects of the adsorber non-isothermality and transport resistances on durations of pressurization and depressurization of the above described zeolite column were

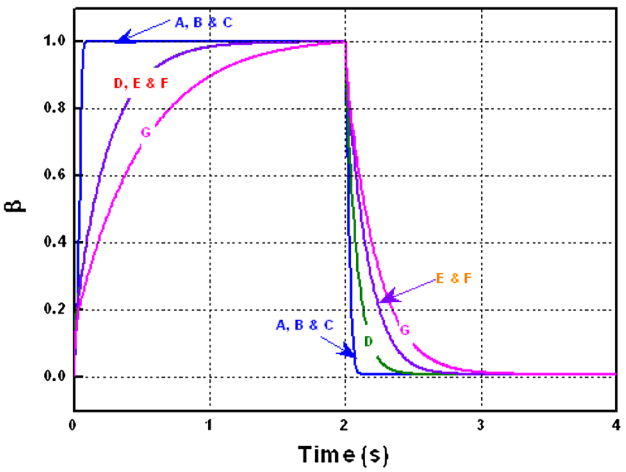

Fig. 4 Influence of various mass, heat and momentum transfer coefficients inside an adsorber column on pressurization-depressurization times using $C_V = 1.5$, $d_p = 400$ μm at $P^o = 4$ atm. A: ideal; B: A + axial dispersion; C: B + heat dispersion; D = C + mass transfer kinetics ($k = 12$ s^{-1}); E: D + pressure drop; F = E + finite heat transfer; G = F + ($k = 6$ s^{-1})

simulated by using the same mathematical model. The adsorber was initially equilibrated with N_2 at ambient pressure and 298 K. It was then pressurized rapidly with pure N_2 from a tank maintained at a super atmospheric pressure level (P^0) through an open valve (valve constant = C_v) until the column pressure reached a value of P^0. The adsorbent temperature rises to T^* during this process. The adsorber was then rapidly depressurized through the same valve until the adsorber pressure reached ambient level. The adsorbent temperature falls back to T^0. The variables for simulation included P^0, C_v, d_p and L/D.

Figure 4 shows a typical example of simulation results for adiabatic pressurization (curves on left) and depressurization (curves on right) of the column ($d_p = 400$ μm, $L/D = 2.5$, $P^0 = 4$ atm, and $C_v = 4$). It plots β which is defined by the fraction of the total amount (adsorbed + void) of N_2 introduced into the column during pressurization ($0 \le \beta \le 1$) or removed from the column during depressurization ($1 \ge \beta \ge 0$) processes as functions of time (t). The LDF mass transfer coefficient was large ($k \sim 12$ s^{-1}).

Curve (A) shows the β profiles for ideal adiabatic pressurization-depressurization steps when instantaneous local equilibrium for both mass and heat exists between the gas and solid phases. Curves (B) and (C) are cases where gas phase axial mass and heat dispersions were added sequentially to case (A). Curve (D) represents the case where adsorption kinetics ($k = 12$ s^{-1}) was added to case (C). It may be seen that curves (A)—(C) are nearly identical for both steps. That is because of small effects of gas phase mass and heat dispersions on these steps. On the other hand, introduction of adsorption kinetics stretches

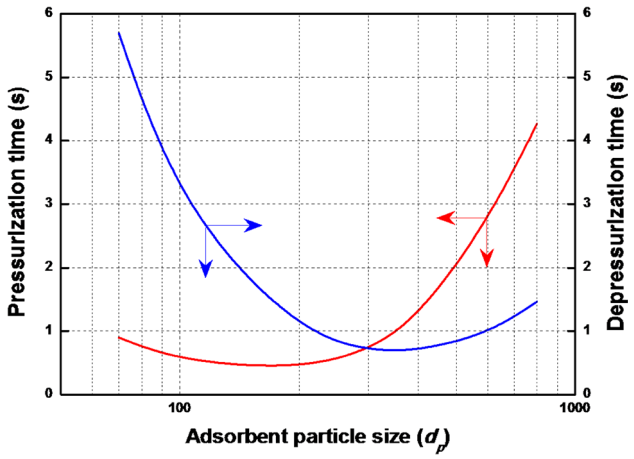

Fig. 5 Simulated base case pressurization—depressurization times as functions of adsorbent particle size (d_p, μm)

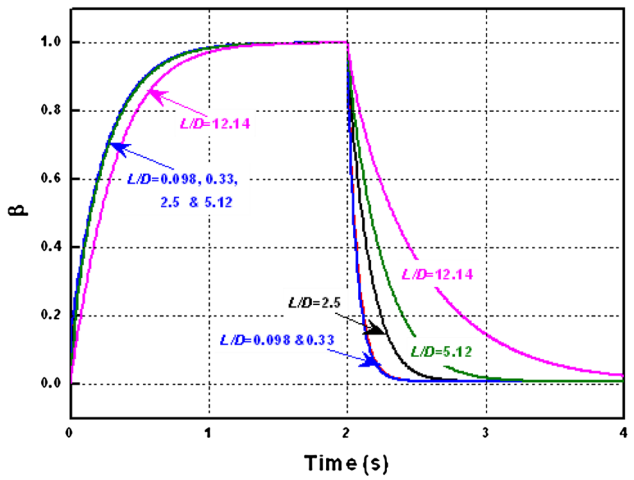

Fig. 6 Influence of column *L/D* on pressurization-depressurization times using $C_V = 4$, $d_p = 400$ μm at $P^o = 4$ atm

both the pressurization and depressurization times. Curve (E) shows the case where column pressure drop was added to case (D). Introduction of column pressure drop further stretches both times, particularly the depressurization time is elongated considerably. Curve (F) of Fig. 4 shows the case where a finite gas–solid heat transfer coefficient was added to the simulation (case E). The effect was negligible. Curve G represents the case where a slower mass transfer coefficient ($k = 6\ s^{-1}$) was used in case E. Slower adsorption kinetics in presence of column pressure drop elongated both times so much that the design of a very rapid PSA cycle may not even be feasible. These observations may be critical issues for design of a practical RPSA process.

The common practice to increase k is to use a smaller d_p. However, smaller d_p increases column pressure drop. These two counteracting effects create a very interesting situation for an optimum d_p as shown by Fig. 5. Durations of <1 s for both steps can be achieved by using a d_p range of ~200–350 μm.

Figure 6 shows the pressurization-depressurization times for the base case adsorber using different *L/D* ratios while having the same *W*. It may be seen that both times increase as the *L/D* increases. The changes in these times for a pancake adsorber ($L/D < 0.2$) are, however small. Each of the steps can be executed in less than 1.2 s provided that $L/D < 2.5$.

The simulations (not shown) also revealed that although the total amount of N_2 in the column at the end of the pressurization (or start of the depressurization) is larger for the isothermal case ($T^0 < T^*$), the times needed for completion of these steps were comparable for both isothermal and adiabatic operations.

3 Summary

It was demonstrated by non-equilibrium, non-isothermal, and non-isobaric, numerical simulations of rapid N_2 desorption from a LiX zeolite column by O_2 purge and rapid pressurization-depressurization of the column using N_2 that adsorption kinetics, adsorber adiabaticity, and column pressure drop play important roles in establishing the efficiency and durations of these processes. Thus, they should be accounted for in a realistic RPSA process model for MOC design. Interestingly many published RPSA process models ignore these issues (Chai et al. 2011). These studies also point out several practical limitations as well as optimum values for (a) total and individual step cycle times (b) adsorbent particle size, and (c) adsorber *L/D* ratio for efficient operation of a RPSA process scheme for MOC application.

References

Chai, S.W., Kothare, M.V., Sircar, S.: Rapid pressure swing adsorption for reduction of bed size factor of a medical oxygen concentrator. Ind. Eng. Chem. Res. **50**, 8703 (2011)

Chai, S.W., Kothare, M.V., Sircar, S.: Numerical study of nitrogen desorption by rapid oxygen purge for a medical oxygen concentrator. Adsorption **18**, 87 (2012)

Chai, S.W., Kothare, M.V., Sircar, S.: Efficiency of nitrogen desorption from LiX zeolite by rapid oxygen purge in a pancake adsorber. AIChE J. **59**, 365 (2013)

Ergun, S.: Fluid flow through packed columns. Chem. Eng. Prog. **48**, 89 (1952)

Leavitt, F.W.: U.S Patent, Air Separation Pressure Swing Adsorption Process, 5, 074, 892 (1991)

Rama Rao, V., Kothare, M.V., Sircar, S.: Numerical simulation of rapid pressurization and depressurization of a zeolite column using nitrogen. Adsorption, DOI 10.1007/s10450-D13-9548-x (2013)

Rege, S.U., Yang, R.T.: Limits for air separation by adsorption with LiX zeolite. Ind. Chem. Eng. Res. **36**, 5358 (1997)

Ruthven, D.M.: Principles of adsorption and adsorption processes. Wiley, New York (1984)
Skarstrom, C.W.: Method and apparatus for fractionating gaseous mixtures by adsorption. U. S. Patent 2,924,627 (1960)
Wakao, N., Kaguei, S., Funazkri, T.: Effect of fluid dispersion coefficients on particle to fluid heat transfer coefficients in packed beds. Chem. Eng. Sci. **34**, 325 (1979)